First-order metal-to-metal phase transition and non-Fermi-liquid behavior in a two-dimensional Mott insulating layer adsorbed on a metal substrate

H. Ishida
College of Humanities and Sciences, Nihon University, Tokyo 156-8550, Japan

A. Liebsch
Peter Grünberg Institut and Institute of Advanced Simulations, Forschungszentrum Jülich, D-52425 Jülich, Germany

(Received 19 August 2011; revised manuscript received 8 November 2011; published 12 January 2012)

The electronic structure of a two-dimensional Mott insulating layer in contact with a semi-infinite metal substrate is studied within cluster dynamical mean field theory. For this purpose, the overlayer forming a square lattice is divided into an array of (2×2)-site clusters in which interatomic electron correlations are taken into account explicitly. In striking contrast to the single-site approximation, where substrate-adsorbate hybridization gives rise to Fermi-liquid properties at low temperature, short-range correlations lead to bad metallicity in a much wider parameter range as a function of temperature and overlayer-substrate coupling strength. The $(\pi,0)$ component of the self-energy exhibits a finite low-energy scattering rate, which increases with decreasing temperature even when hybridization between overlayer and substrate states is as large as the nearest-neighbor hopping energy within the overlayer. In addition, at moderate overlayer-substrate coupling and in the presence of the second nearest-neighbor hopping interaction, the overlayer undergoes a first-order phase transition between two correlated metallic phases when electron doping is increased by changing the chemical potential. These results suggest that normal metal proximity effects are strongly modified when spatial fluctuations in the overlayer are taken into consideration.

DOI: 10.1103/PhysRevB.85.045112 PACS number(s): 73.20.−r, 73.40.Ns, 71.27.+a, 71.10.Hf

I. INTRODUCTION

Heterostructures made out of atomically controlled thin layers of strongly correlated materials are currently a topic of intense study.[1–11] Due to various effects peculiar to multilayer systems, such as electron confinement and charge transfer across the interface, they exhibit novel properties absent in the constituent bulk materials. From the viewpoint of device applications, an important question arises as to whether nanoscale devices, such as tunneling junctions, function in the same manner when conventional band insulators like magnesium or silicon oxides are replaced by insulators associated with strong Coulomb interactions. In order to answer this question, it is crucial to understand the electronic properties of the interface between a weakly correlated metal and a Mott insulator.

On the theory side, several authors addressed this issue by applying dynamical mean-field theory (DMFT)[12,13] to Hubbard-type model Hamiltonians with a layer-dependent Coulomb repulsion. Helmes *et al.*[14] considered the planar interface between a semi-infinite metal and a semi-infinite Mott insulator (or bad metal) for half-filled electron-hole symmetric systems at very low temperatures. They showed that a quasiparticle peak characteristic of metallic states appears in the one-electron excitation spectra of the insulating layers via the Kondo proximity effect and that its spectral weight drops rapidly with increasing distance from the metal. Zenia *et al.*[15] considered a finite number of Mott insulating layers sandwiched between two metal electrodes. They characterized the metallic state in the insulating barrier region induced by the metal proximity effect at low temperatures as a "fragile" Fermi liquid and suggested the possibility of utilizing such a quantum state for nonlinear devices. Both studies adopted the "inhomogeneous" layer DMFT approach of Potthoff and Nolting[16] in which the electron self-energy is assumed to be local in real space and its layer dependence is determined self-consistently by solving a coupled DMFT equation.

To examine nonlocal self-energy effects in correlated heterostructures, caused by short-range spatial fluctuations ignored in previous single-site DMFT calculations, we recently considered two- and three-layer-thick insulator films sandwiched between two metals,[17] where interatomic Coulomb correlations were treated within the cluster extension of DMFT.[18] As the numerical effort increases exponentially with cluster size, one-dimensional atomic chains oriented normal to the interface plane were chosen as cluster units, so that interlayer electron correlations are fully taken into account while intralayer fluctuations are ignored. The system was assumed to be half-filled and electron-hole symmetric, and its electronic structure was evaluated as a function of the on-site Coulomb repulsion energy. The important result of this study was that the mechanism by which the metallic states penetrate the insulating film depends significantly on the electronic structure of the isolated film. For instance, in the case of a double-layer system, the quasiparticle peak, which appears within single-site DMFT via the Kondo proximity effect,[14,15] is absent when interplanar correlations are taken into account. The origin of this striking difference was shown to be associated with different mechanisms for the metal-insulator transition. Within single-site DMFT, the Mott gap opens because of the divergence of the local self-energy; within the cluster DMFT, the gap opens via a discontinuous change in the real part of the interlayer component of the self-energy. These results underline the importance of appropriately considering interatomic Coulomb correlations in describing the electronic structure of strongly correlated heterostructures.

In the present work, we explore another aspect of the electronic structure of metal-insulator interfaces by

incorporating intraplanar Coulomb correlations that were disregarded previously.[17] To be specific, we consider an insulating monolayer described by the two-dimensional (2D) Hubbard model and investigate its interaction with a noninteracting semi-infinite metal substrate. Because of the relevance for cuprate high-T_c superconductors, a number of groups applied cluster extensions of DMFT to the single-band Hubbard model for a 2D square lattice.[19–28] These works greatly revised the earlier understanding of this system within single-site DMFT, with regard to both the nature of the metal-insulator transition and the overall shape of the phase diagram. Moreover, they revealed that intersite correlations give rise to a pronounced momentum-space anisotropy of the gap opening and to the appearance of non-Fermi-liquid properties as a function of electron and hole doping concentrations. It is therefore intriguing to study how these properties are modified when the correlated 2D layer is attached onto a metallic substrate. The Coulomb energy of the system is chosen such that the isolated monolayer is a Mott insulator. Its electronic properties are then studied by varying the hybridization to the metallic substrate, the electron chemical potential, and the temperature.

The main results of this work are as follows: (i) When the overlayer is coupled to the substrate via orbital hybridization, the overlayer exhibits bad-metallic rather than Fermi-liquid properties as a result of short-range correlations in a much wider parameter range than expected from single-site DMFT calculations. In particular, the self-energy component of the cluster corresponding to the $(\pi,0)$ point of the 2D Brillouin zone exhibits strong bad-metallic behavior even when orbital mixing between the overlayer and substrate states is as large as the nearest-neighbor hopping interaction within the overlayer. (ii) On the electron doping side, the first-order metal-to-insulator transition of the isolated monolayer in the presence of second-neighbor hopping interactions becomes a first-order phase transition between strongly and weakly correlated metallic phases. These results reveal that the normal metal proximity effect is strongly reduced when short-range interatomic correlations within the overlayer are incorporated.

The outline of this paper is as follows. In Sec. II, we describe the present model and discuss several theoretical details of the cluster DMFT calculations. In Sec. III, we present the numerical results and clarify how the Mott insulator is metallized when it is coupled with the metal substrate via orbital hybridization. Section IV contains the summary. The Appendix summarizes the main results for the same system obtained within the single-site DMFT.

II. THEORY

As shown in Fig. 1, we consider an interface system in which a monolayer of interacting electrons on a square lattice is adsorbed on top of a semi-infinite metal substrate of noninteracting electrons on a simple-cubic lattice. The Hamiltonian consists of three parts,

$$\hat{H} = \hat{H}_a + \hat{H}_s + \hat{H}_{as}, \tag{1}$$

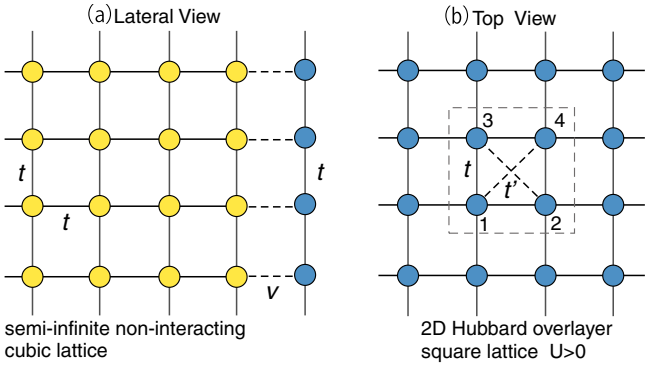

FIG. 1. (Color online) Tight-binding model for an insulating monolayer on top of a semi-infinite metal. (a) Lateral view; (b) top view. The four-site cluster indicated by a dashed square is used as a unit in the cluster DMFT calculation.

where the Hamiltonian of the isolated monolayer, $\hat{H}_a$, is given by the Hubbard model for a 2D square lattice,

$$\hat{H}_a = -\sum_{ij\sigma} t_{ij} c^\dagger_{i\sigma} c_{j\sigma} + U \sum_i \left(\hat{n}_{i\uparrow} - \frac{1}{2}\right)\left(\hat{n}_{i\downarrow} - \frac{1}{2}\right). \tag{2}$$

Here, $\hat{n}_{i\sigma} = c^\dagger_{i\sigma} c_{i\sigma}$ denotes the electron occupation on overlayer site i with spin $\sigma = \uparrow, \downarrow$ and U is the on-site Coulomb repulsion energy. In the summation in the first term of Eq. (2), we include first and second nearest-neighbor hopping interactions, t and t'. Thus, the band dispersion of the isolated film is given by $\epsilon(\mathbf{k}) = \epsilon_t(\mathbf{k}) - 4t' \cos(k_x)\cos(k_y)$, where $\epsilon_t(\mathbf{k}) \equiv -2t[\cos(k_x) + \cos(k_y)]$. The x and y axes are parallel to the two principal directions of the square lattice. The lattice constant is chosen as unity, so that $-\pi \leqslant k_x, k_y \leqslant \pi$. The second nearest-neighbor interaction, t', introduces asymmetry between the hole and electron doping regions.

The Hamiltonian of the metal substrate is given by

$$\hat{H}_s = -\sum_{mn\sigma} t\, a^\dagger_{m\sigma} a_{n\sigma}, \tag{3}$$

where $a_{m\sigma}$ is the electron annihilation operator for substrate site m and spin σ. Since the role of the substrate is to broaden the one-electron spectra of the overlayer, we consider only electron hoppings between first nearest neighbors. To reduce the number of parameters, the hopping integral is assumed to be the same in the overlayer, so that the substrate represents a metal with bandwidth $W = 12t$. For each 2D momentum $\mathbf{k}$, the energy continuum of the substrate extends over a region of width $4t$ and whose center is located at $\epsilon_t(\mathbf{k})$. Thus, as long as $|t'| < |t|/2$, the overlayer energy band hybridizes with the substrate energy continuum throughout the whole surface Brillouin zone.

$\hat{H}_{as}$ in Eq. (1) represents the orbital coupling between substrate and overlayer states,

$$\hat{H}_{as} = -\sum_{im\sigma} v(c^\dagger_{i\sigma} a_{m\sigma} + \text{H.c.}), \tag{4}$$

where the parameter v controls the hybridization strength, and the summation is taken over all pairs of atomic sites in the overlayer and their nearest neighbors in the outermost layer of the substrate.

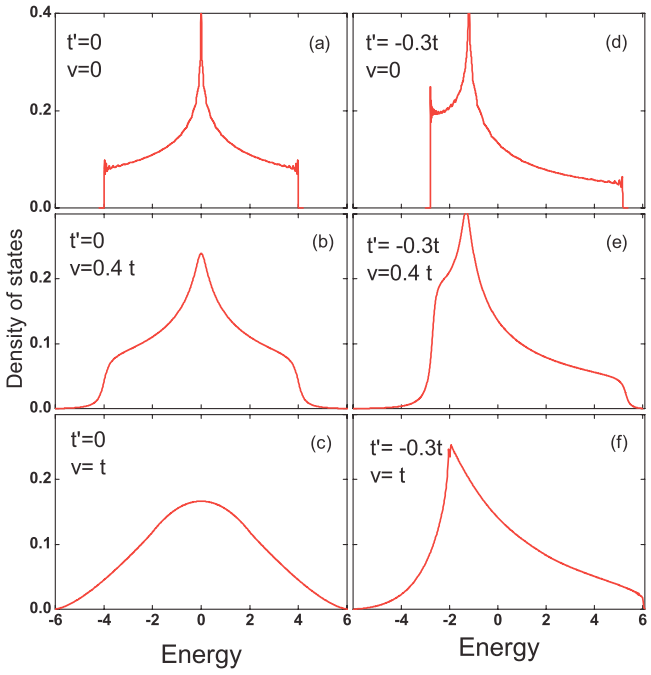

FIG. 2. (Color online) Density of states of noninteracting electrons projected on an overlayer site for several values of t', second-neighbor hopping interaction in the overlayer, and v, mixing parameter between overlayer and substrate sites.

Figure 2 shows the density of states (DOS) of noninteracting electrons ($U = 0$) projected on an overlayer site for three values of v. The left panels correspond to $t' = 0$, while the right panels correspond to $t' = -0.3t$. The latter value was used in the past to simulate normal-state properties of high-T_c cuprates.[19,20,26] As expected, the van Hove singularity characterizing the DOS of the square lattice becomes rapidly smeared out with increasing orbital mixing v and the bandwidth increases from $8t$ to $12t$. Accordingly, the left bottom panel for $t' = 0$ and $v = t$ represents the DOS of the top layer of a semi-infinite simple-cubic lattice with bandwidth $W = 12t$.

To apply the cluster DMFT formalism,[18] the overlayer is divided into four-site clusters forming a 2×2 superlattice as shown in Fig. 1, where site labels refer to $1 \equiv (0,0), 2 \equiv (1,0)$, $3 \equiv (0,1)$, and $4 \equiv (1,1)$. To avoid confusion, we use in the following the notation in which a matrix is expressed as $\hat{A}$ and its elements as A_{ij}. The interacting lattice Green's function at finite temperature T in the cluster-site basis is written as

$$\hat{G}(i\omega_n) = \sum_{\mathbf{k}'} [i\omega_n + \mu - \hat{t}(\mathbf{k}') - \hat{\Sigma}(i\omega_n) - \hat{s}(\mathbf{k}', i\omega_n + \mu)]^{-1}, \tag{5}$$

where the sum over $\mathbf{k}'$ extends across the reduced Brillouin zone, $-\pi/2 \leqslant k'_x, k'_y \leqslant \pi/2$, $\omega_n = (2n+1)\pi T$ are Matsubara frequencies, $\hat{t}(\mathbf{k}')$ denotes the hopping matrix for the superlattice, and $\hat{\Sigma}(i\omega_n)$ is the self-energy matrix accounting for electron correlations. Among the 16 elements of $\hat{G}$, only three, namely G_{11}, G_{12}, and G_{14}, are the independent because of symmetry. We restrict ourselves to paramagnetic solutions and omit spin indices in the equations hereafter.

The quantity $\hat{s}(\mathbf{k}', z)$ in Eq. (5) denotes the embedding potential at complex energy z and describes the hybridization effect of the semi-infinite substrate on the overlayer,[29,30]

$$s_{ij}(\mathbf{k}', z) = \frac{v^2}{4} \sum_{\mathbf{p}} e^{i\mathbf{p}\cdot(\mathbf{x}_i - \mathbf{x}_j)} g_{00}\left[z - \epsilon_t(\mathbf{p})\right], \tag{6}$$

where $\mathbf{x}_i$ is the 2D coordinate of site i ($1 \leqslant i \leqslant 4$), the summation is taken over four wave vectors, $\mathbf{p} = \mathbf{k}' + (m,n)\pi$, with m,n being 0 or 1, and g_{00} denotes the surface component of the Green's function of a semi-infinite tight-binding chain with first neighbor hopping integral, $-t$,[31]

$$g_{00}(w) = \frac{w - \sqrt{w^2 - 4t^2}}{2t^2}. \tag{7}$$

The overlayer Green's function and self-energy matrices become diagonal when expressed in the molecular orbital basis defined by[26]

$$\begin{aligned} |\Gamma\rangle &= \tfrac{1}{2}\left(|1\rangle + |2\rangle + |3\rangle + |4\rangle\right), \\ |\mathrm{M}\rangle &= \tfrac{1}{2}\left(|1\rangle - |2\rangle - |3\rangle + |4\rangle\right), \\ |\mathrm{X}\rangle &= \tfrac{1}{2}\left(|1\rangle - |2\rangle + |3\rangle - |4\rangle\right), \\ |\mathrm{Y}\rangle &= \tfrac{1}{2}\left(|1\rangle + |2\rangle - |3\rangle - |4\rangle\right). \end{aligned} \tag{8}$$

Physically, $|\Gamma\rangle$, $|\mathrm{M}\rangle$, $|\mathrm{X}\rangle$, and $|\mathrm{Y}\rangle$ can be regarded as representing a coarse-grained approximation around the $(0,0)$, (π,π), $(\pi,0)$, and $(0,\pi)$ points of the Brillouin zone, respectively. The diagonal elements of the Green's function in this molecular orbital basis are related to the three independent elements of the Green's function in the site basis via

$$\begin{aligned} G_\Gamma &= G_{11} + 2G_{12} + G_{14}, \\ G_\mathrm{M} &= G_{11} - 2G_{12} + G_{14}, \\ G_\mathrm{X} &= G_\mathrm{Y} = G_{11} - G_{14}. \end{aligned} \tag{9}$$

Analogous relationships hold for the self-energy matrix. The bath Green's function determining the Weiss mean-field Hamiltonian is obtained by removing the self-energy matrix from the lattice Green's function:

$$\hat{G}^0(i\omega_n) = [\hat{G}^{-1}(i\omega_n) + \hat{\Sigma}(i\omega_n)]^{-1}, \tag{10}$$

which is also diagonal in the molecular orbital representation.

The quantum impurity problem is solved by making use of the exact diagonalization (ED) formalism.[32] Its applicability has recently been extended to multisite and multiorbital systems at finite temperatures.[33–35] To implement this method, each diagonal component of $\hat{G}^0$ is approximated via a noninteracting Green's function of a finite system consisting of a single impurity level with energy E_m and n_b bath orbitals with energy ϵ_{mk}. Thus,

$$\begin{aligned} G^0_m(i\omega_n) &\approx G^{cl,0}_m(i\omega_n) \\ &= \left(i\omega_n + \mu - E_m - \sum_{k=1}^{n_b} \frac{|v_{mk}|^2}{i\omega_n - \epsilon_{mk}}\right)^{-1}, \end{aligned} \tag{11}$$

where m denotes one of the molecular orbitals. The $(2n_b + 1)$ fitting parameters, E_m, ϵ_{mk}, and v_{mk}, are chosen such that the quantities

$$F_m = \sum_{n=0}^{n_{\max}} \left| G_m^0(i\omega_n) - G_m^{cl,0}(i\omega_n) \right|^2 / \omega_n \qquad (12)$$

are minimized. Returning from the molecular orbital basis to the site basis by a unitary transformation, we now obtain the Hamiltonian for a larger cluster consisting of the four square sites and the $4n_b$ bath levels. After adding the on-site Coulomb repulsion terms to this $4(1 + n_b)$-level cluster, the lowest eigenstates relevant at temperature T are calculated by using the Arnoldi algorithm.[36] The interacting cluster Green's function, $\hat{G}^{\rm cl}$, is then derived via the Lanczos procedure. Finally, the cluster self-energy is obtained from an expression analogous to Eq. (10):

$$\hat{\Sigma}^{\rm cl}(i\omega_n) = [\hat{G}^{\rm cl,0}(i\omega_n)]^{-1} - [\hat{G}^{\rm cl}(i\omega_n)]^{-1}. \qquad (13)$$

In the molecular orbital basis, this self-energy is also diagonal.

In the ED cluster DMFT formalism, the cluster self-energy is assumed to be a physically reasonable representation of the lattice self-energy. Thus, $\hat{\Sigma}^{\rm cl}(i\omega_n)$ is used as the input self-energy in Eq. (5) for the next iteration. This procedure is iterated until the difference between the input and output self-energy matrices becomes sufficiently small. More details of the calculational method are given in Ref. 33. Note that, since the self-energy is nondiagonal in the site representation, all its elements contribute in a highly nonlinear manner to all lattice Green's function components.

In the calculations discussed below, we use $n_b = 2$ bath orbitals per molecular orbital component. Thus, the total number of levels in the ED cluster is $n_s = 4(1 + n_b) = 12$. While this number may appear relatively small, due to the indirect Coulomb coupling between bath levels the spacing between cluster excitation energies is very small, so that an accurate evaluation of the Green's function is feasible, even at rather low temperatures.

III. RESULTS AND DISCUSSION

As we are interested in the metallization of the Mott insulating layer, we choose the on-site Coulomb repulsion energy as $U = 9t$, such that the isolated layer at half-filling is a Mott insulator.[21] For clarity, we begin the discussion with the case of the symmetric noninteraction DOS with $t' = 0$. The results for the electron-hole asymmetric systems with nonvanishing t' will be presented in Sec. III D. For completeness, analogous results derived within single-site DMFT are summarized in the Appendix.

A. Electron occupation and spectral weight at chemical potential: Metallization of the overlayer

Figure 3(a) shows the electron occupation per spin of an overlayer site as a function of chemical potential μ. To illustrate the effect caused by hybridization between overlayer and substrate, the results are shown for three coupling strengths: $v = 0$, $v = 0.8t$, and $v = t$. As we consider the case $t' = 0$, the condition $n(\mu) = 1 - n(-\mu)$ holds. In the case of the isolated monolayer ($v = 0$), the occupation

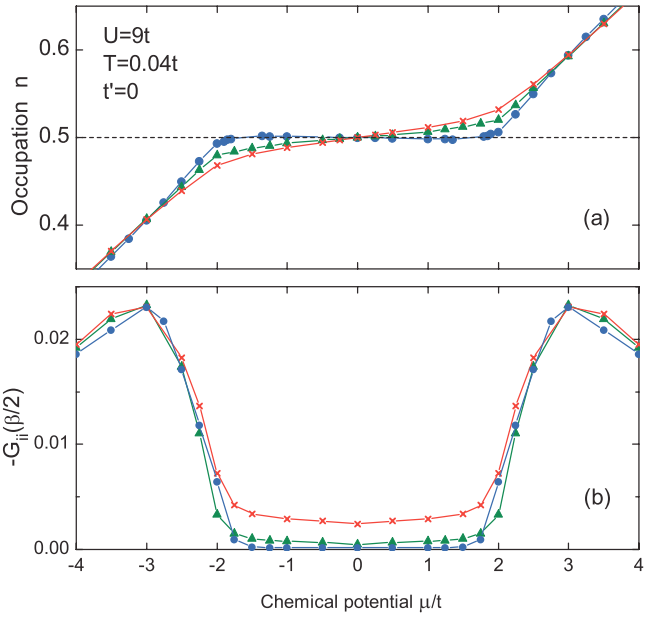

FIG. 3. (Color online) (a) Electron occupation per spin and (b) integrated spectral weight around chemical potential, $-G_{ii}(\beta/2)$, of an overlayer site as a function of chemical potential μ derived within four-site cluster DMFT. $U = 9t$, $T = 0.04t$, and $t' = 0$. Filled circles, triangles, and crosses correspond to substrate-adatom hybridizations, $v = 0$, $v = 0.8t$, and $v = t$, respectively.

exhibits a plateau, $n(\mu) = 0.5$, in the interval $\mu_h \leqslant \mu \leqslant \mu_e$, with $|\mu_h| = |\mu_e| \approx 2t$, which marks the appearance of the Mott insulating phase. Moreover, within the accuracy of our calculations, $n(\mu)$ does not indicate a discontinuous change at the critical μ values, so that the metal-insulator phase transition for $t' = 0$ is continuous.

When the overlayer substrate interaction is switched on, the plateau in $n(\mu)$ disappears and the compressibility $(dn/d\mu)_T$ is positive in the entire μ range, indicating that the overlayer is now metallic. Thus, as a result of the proximity effect, metallic substrate states leak into the strongly correlated overlayer. Nevertheless, as seen from Fig. 3(a), the slope of $n(\mu)$ in the range of the original Mott gap for $v = 0.8t$ and $v = t$ is considerably smaller than beyond this region.

The metal-insulator transition of the isolated monolayer as a function of μ can also be studied by monitoring the quasiparticle DOS at the chemical potential. A convenient quantity for this purpose is the imaginary-time Green's function at $\tau = \beta/2$, which is related to the quasiparticle DOS via

$$G_{ii}(\beta/2) = -\int_{-\infty}^{\infty} d\omega\, F(\omega)\, \rho_i(\omega,\mu), \qquad (14)$$

where $F(\omega) = 0.5/\cosh[(\beta\omega)/2]$ is a distribution of width $4\ln(2 + \sqrt{3})/\beta$ centered about $\omega = 0$, and the quasiparticle DOS of site i ($i = 1$ to 4) is defined by

$$\rho_i(\omega,\mu) = -\frac{1}{\pi}{\rm Im}G_{ii}(\omega + i\delta), \qquad (15)$$

with a positive infinitesimal δ. $-G_{ii}(\beta/2)$ represents the integrated spectral weight within a few T around the electron chemical potential.

In Fig. 3(b), we show $-G_{ii}(\beta/2)$ of an overlayer site as a function of μ for $v = 0$, $v = 0.8t$, and $v = t$. It is seen that $-G_{ii}(\beta/2)$ of the isolated monolayer (filled circle) vanishes inside the energy gap. Because of the broadening factor $F(\omega)$ in Eq. (14), $-G_{ii}(\beta/2)$ does not drop to zero abruptly at the metal-insulator phase boundaries, so that the energy gap in Fig. 3(b) appears to be somewhat narrower than the width of the plateau in Fig. 3(a).

Triangles and crosses in Fig. 3(b) show $-G_{ii}(\beta/2)$ for $v = 0.8t$ and $v = t$, respectively. In the μ range beyond the original Mott gap ($|\mu| > |\mu_{e(h)}|$), $-G_{ii}(\beta/2)$ is seen to be rather insensitive to the mixing parameter v. On the other hand, upon metallization, $-G_{ii}(\beta/2)$ in the original Mott gap takes positive values. However, it is seen that $-G_{ii}(\beta/2)$ in this range grows only a little up to $v = 0.8t$. Then, it begins to increase more rapidly between $v = 0.8t$ and t. Together with the smaller slope of $(dn/d\mu)_T$ as discussed above, this is clear evidence that the metallic phase in the original Mott gap is much more strongly correlated than the metallic phases in the outer regions. As will be discussed in the next subsection, in striking contrast to the single-site DMFT calculation for the metal/Mott insulator interface[14,15] (see also the Appendix), the metallized overlayer in the cluster DMFT treatment becomes a bad metal instead of a Fermi liquid in a wide parameter range as a function of T, μ, and v. In particular, the large amplitude of the imaginary part of the self-energy of the X orbital results in a strong reduction of the quasiparticle DOS at the chemical potential, as seen in Fig. 3(b). This is in contrast to the single-site DMFT, where $-G_{ii}(\beta/2)$ in the original Mott gap region grows rapidly upon switching on the mixing parameter v due to a formation of the quasiparticle DOS peak at μ (see Fig. 16 in the Appendix).

To gain more insight into the electronic structure of the overlayer, we calculate the nonlocal spin correlations characterized by $\chi_{ij}(\tau) = \langle \hat{s}_{zi}(\tau)\hat{s}_{zj}(0) + \hat{s}_{zj}(\tau)\hat{s}_{zi}(0)\rangle/2$, where τ denotes imaginary time, and i and j are site indices in the 2×2 cluster. In Fig. 4, we show the nearest-neighbor element of the spin correlation function at $\tau = 0$, $\chi_{12}(\tau = 0)$, as a function of μ for the same parameter set as that in Fig. 3. For comparison, we also plot $\chi_{12}(0)$ of a weakly correlated isolated monolayer with $U = 4t$ and $v = 0$. By comparing the filled and open circles, we realize that the Mott insulating phase

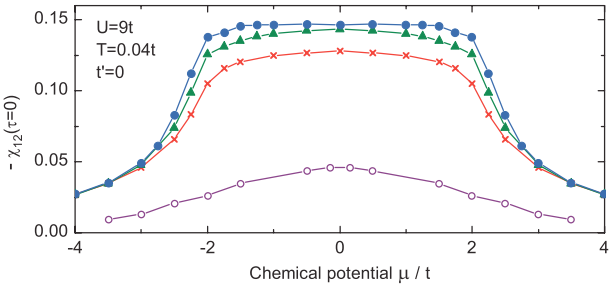

FIG. 4. (Color online) $\chi_{12}(\tau = 0)$, nearest-neighbor spin correlation at imaginary time $\tau = 0$ as a function of μ derived within four-site cluster DMFT. $U = 9t$, $T = 0.04t$, and $t' = 0$. Filled circles, triangles, and crosses correspond to substrate-adatom hybridizations, $v = 0$, $v = 0.8t$, and $v = t$, respectively. For comparison, we also show $\chi_{12}(\tau = 0)$ of a weakly correlated isolated monolayer with $U = 4t$ and $v = 0$ (open circles).

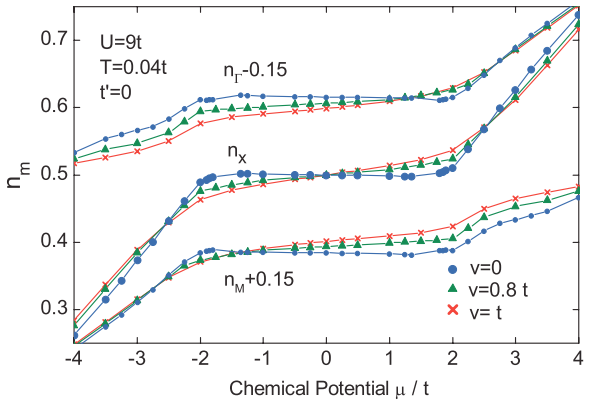

FIG. 5. (Color online) Molecular orbital occupations per spin as functions of chemical potential. $U = 9t$, $T = 0.04t$, and $t' = 0$. $v = 0$ (filled circle), $v = 0.8t$ (triangle), and $v = t$ (cross). For clarity, $n_\Gamma(\mu)$ and $n_M(\mu)$ are shifted vertically by ∓ 0.15.

($v = 0$) is characterized by nearly constant and large negative values of $\chi_{12}(0)$, which implies a strong tendency toward antiferromagnetic ordering of nearest-neighbor electron spins. Interestingly, this negative amplitude of $\chi_{12}(0)$ decreases only modestly for the metallized overlayers with $v = 0.8t$ and $v = t$, indicating that the electron motion in the overlayer is strongly correlated for these orbital mixing parameters.

We have also analyzed the contributions of each molecular orbital to the total occupancy, $n_m(\mu)$, since they play distinct roles in the Mott transition and non-Fermi-liquid properties of the isolated monolayer.[21,26] Figure 5 shows the orbital occupations $n_m(\mu)$ as functions of chemical potential for three interaction strengths. It is seen that for $v = 0.8t$ and $v = t$, $(dn_m/d\mu)_T$ is positive in the region of the Mott gap of the isolated monolayer, indicating that all molecular orbitals take part in the metallization of the overlayer.

B. Adsorbate self-energy in cluster DMFT: Bad-metallic properties

Although the dependency of the electron occupation and the integrated DOS around chemical potential on various system parameters provides important information on the nature of the electronic phase transitions in the overlayer, additional aspects, such as deviations from Fermi-liquid behavior, can be derived by analyzing the energy dependence of the self-energy.

Figure 6 shows the real and imaginary parts of the self-energy of the Γ and M orbitals at the first Matsubara frequency $\omega_0 = \pi T$ as a function of μ. The parameters are the same as in Fig. 3, i.e., $U = 9T$ and $T = 0.04t$, with adatom-substrate orbital mixing $v = 0$ (filled circle), $v = 0.8t$ (triangle), and $v = t$ (cross). For comparison, panel (a) also shows the corresponding results for a weakly correlated isolated monolayer with $U = 4t$ and $v = 0$ (open circle). In this case, the monolayer remains a Fermi liquid in the entire μ range, and the self-energies of both orbitals are nearly degenerate.

Consider first the case $v = 0$. As discussed in the preceding subsection, the isolated monolayer is an insulator for $\mu_h \leqslant \mu \leqslant \mu_e$. It is seen from Fig. 6(a) that the metal-insulator transition on the hole doping side is characterized by a steep

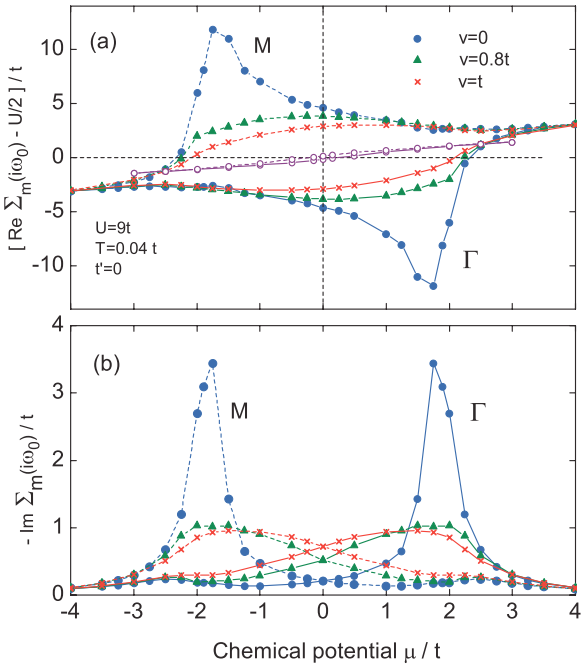

FIG. 6. (Color online) (a) Real and (b) imaginary parts of the self-energy of the Γ and M orbitals at the first Matsubara frequency $\omega_0 = \pi T$ for $v = 0$ (filled circle), $v = 0.8t$ (triangle), and $v = t$ (cross). $U = 9t$, $T = 0.04t$, and $t' = 0$. Solid and dashed lines correspond to the Γ and M orbitals, respectively. In (a), we also show by open circles the self-energy of both orbitals for a weakly correlated isolated monolayer with $U = 4t$ and $v = 0$.

increase in $\mathrm{Re}\Sigma_{\mathrm{M}}(i\omega_0)$ with increasing μ at around $\mu \approx -2t$, which pushes aside the major part of the M band to energies above μ. It should still be noted that the M band is not completely emptied, as seen from Fig. 5. Also, since the phase transition on the hole doping side is continuous, while $\mathrm{Re}\Sigma_{\mathrm{M}}(i\omega_0)$ increases quite steeply at $\mu \approx -2t$, it exhibits no discontinuous change at the critical value μ_h. As a result of the Kramers-Kronig relation for the self-energy as a function of frequency, a similar behavior is found also as a function of the chemical potential μ. Thus, the steep increase in $\mathrm{Re}\Sigma_{\mathrm{M}}(i\omega_0)$ results in a sharp peak structure emerging in the imaginary part of $\Sigma_{\mathrm{M}}(i\omega_0)$ at $\mu \approx -2t$, as seen in Fig. 6(b). In the same way, the metal-insulator transition on the electron doping side is caused by a steep decrease in $\mathrm{Re}\Sigma_{\Gamma}(i\omega_n)$ with decreasing μ at $\mu \approx 2t$, which pulls down the major part of the Γ band toward energies below μ. Correspondingly, $\mathrm{Re}\Sigma_{\Gamma}(i\omega_0)$ exhibits a sharp peak structure at $\mu \approx 2t$.

We conclude from Fig. 6 that the insulating phase for the isolated monolayer is characterized by a large splitting of the real part of the self-energies of the Γ and M orbitals, including the special case of the metal-insulator transition at $\mu = 0$ in the U-T phase diagram studied by Park *et al.*[21] On the other hand, in the outer region of μ where electrons or holes are doped into the monolayer, the self-energies of both orbitals become nearly degenerate.

Let us now consider the effect of finite overlayer-substrate coupling. The triangles and crosses in Fig. 6(a) show the real part of the self-energy of the Γ and M orbitals for two orbital mixing parameters, $v = 0.8t$ and $v = t$, respectively. For these values of v, the overlayer is metallized in the whole μ range. It is seen that the splitting of the real part of the two self-energy components is reduced with increasing v. In particular, the steep rise and the maximum in $\mathrm{Re}\Sigma_{\mathrm{M}}(i\omega_0)$ at $\mu \approx -2t$ for $v = 0$ and the corresponding minimum in the Γ orbital at $\mu \approx 2t$ disappear. Simultaneously, due to the Kramers-Kronig relation, the sharp peak at around μ_h (μ_e) in $\mathrm{Im}\Sigma_{\mathrm{M}(\Gamma)}(i\omega_0)$ degrades to a broad structure with increasing v. Nevertheless, even for these v values, the splitting of the real part of both components is much larger than that of the weakly correlated monolayer shown by open circles in panel (a), indicating that the overlayer is strongly correlated up to large v values.

To examine whether the Γ and M orbitals contribute to the non-Fermi-liquid properties of the metallized overlayer, we plot in Fig. 7 the imaginary part of the self-energy of both orbitals as a function of Matsubara frequency ω_n. Here we have chosen a lower temperature $T = 0.01t$ rather than $T = 0.04t$ in Fig. 6 to better see the behavior of the self-energy in the low ω_n limit. In panel (a), we show $\mathrm{Im}\Sigma_{\Gamma,\mathrm{M}}$ (degenerate) for the electron-hole symmetric case at $\mu = 0$ for four values of the orbital mixing parameter v. While the isolated monolayer with $v = 0$ is insulating, $\mathrm{Im}\Sigma_{\Gamma,\mathrm{M}}$ is linear in ω_n as $\omega_n \to 0$, confirming that the metal-insulating transition for $v = 0$ is associated with the splitting of the real part of the two self-energy components, as discussed above. Although the results

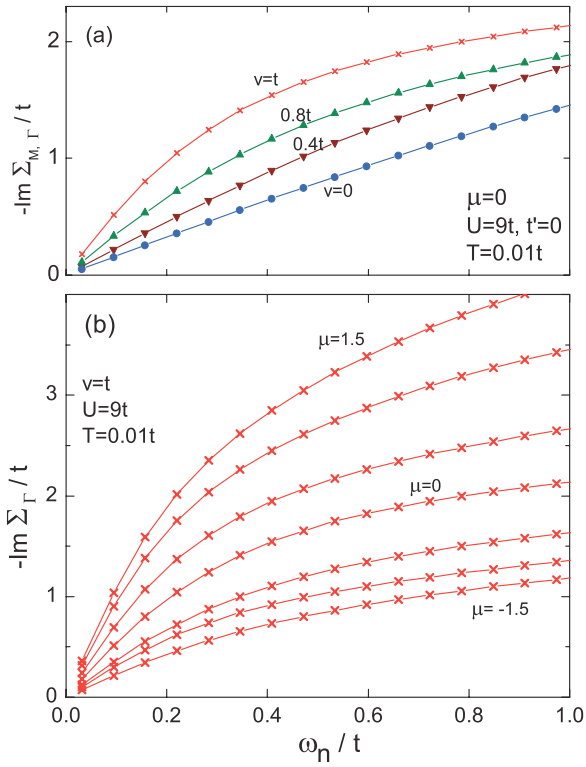

FIG. 7. (Color online) Imaginary part of the self-energy of the Γ and M orbitals as a function of Matsubara frequencies ω_n for $U = 9t$ and $T = 0.01t$. Panel (a) shows the electron-hole symmetric case with $\mu = 0$ for four values of the mixing parameters v. Note that both components are degenerate at $\mu = 0$. Panel (b) shows the μ dependence of $\mathrm{Im}\Sigma_{\Gamma}$ for the largest orbital hybridization parameter $v = t$. μ increases from $-1.5t$ (bottom) to $1.5t$ (top) at intervals of $0.5t$. $\mathrm{Im}\Sigma_{\mathrm{M}}$ for μ coincides with $\mathrm{Im}\Sigma_{\Gamma}$ for $-\mu$.

in Fig. 6(b) might suggest that $\mathrm{Im}\Sigma_{\Gamma,\mathrm{M}}(i\omega_0)$ for $T = 0.04t$ have finite values in the limit of $\omega_n \to 0$, this is caused by the relatively large ω_0 value for $T = 0.04t$. As may be seen from Fig. 7(a), $\mathrm{Im}\Sigma_{\Gamma,\mathrm{M}}(i\omega_n)$ at a lower temperature $T = 0.01t$ actually remains $\sim\omega_n$ in the low ω_n limit even when the orbital hybridization is switched on by increasing v.

We have also studied to what extent the low-frequency behavior of the imaginary part of the self-energy of the two orbitals varies with μ. As seen from Fig. 6(b), $\mathrm{Im}\Sigma_{\Gamma(\mathrm{M})}(i\omega_0)$ of the isolated overlayer with $v = 0$ exhibits a large peak at $\mu \approx 2t$ $(-2t)$, which means that the Γ (M) orbital possesses a finite scattering rate in the low-frequency limit around $\mu \approx 2t(-2t)$. In contrast, with increasing v, the imaginary part of their self-energies gradually changes to a linear function with ω_n. To demonstrate this, we show in Fig. 7(b) the $\mathrm{Im}\Sigma_\Gamma$ curves for the largest orbital mixing parameter $v = t$ and for μ in the range between $-1.5t$ and $1.5t$, all of which tend to 0 in the low-frequency limit. From Fig. 7 one may safely say that the Γ and M orbitals do not contribute to the non-Fermi-liquid properties of the metallized overlayer.

Next, we discuss the self-energy of the X orbital, which exhibits more complex behavior than the Γ and M orbitals. Moreover, it is responsible for the non-Fermi-liquid properties of the metallized overlayer. The filled circles in Figs. 8(a) and 8(b) show the real and imaginary parts of the self-energy of the X orbital at the first Matsubara frequency $\omega_0 = \pi T$ as a function of μ for the isolated monolayer with $v = 0$ at $T = 0.04t$. As is known, for the half-filled insulating system with $\mu = 0$ and $v = 0$, the self-energy of the X orbital diverges at low ω_n as

$$\Sigma_{\mathrm{X}}(i\omega_n) \simeq \frac{U}{2} + \frac{A}{i\omega_n}, \tag{16}$$

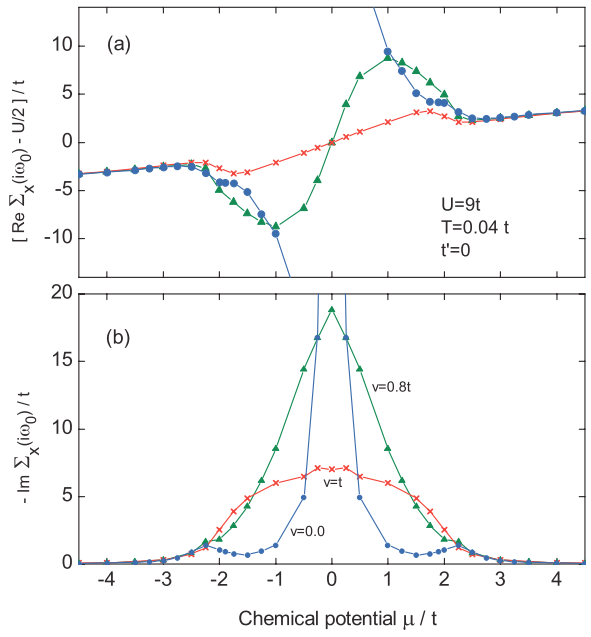

FIG. 8. (Color online) (a) Real and (b) imaginary parts of the self-energy of the X orbital at the first Matsubara frequency $\omega_0 = \pi T$ for $v = 0$ (filled circle), $v = 0.8t$ (triangle), and $v = t$ (cross). $U = 9t$, $T = 0.04t$, and $t' = 0$.

with a positive constant A.[21] For finite but small values of μ, the variation of $\Sigma_{\mathrm{X}}(i\omega_0)$ of the isolated monolayer as a function of μ in Fig. 8 may be understood in terms of a resonance form,

$$\Sigma_{\mathrm{X}}(i\omega_n) \simeq \frac{U}{2} + \frac{A}{i\omega_n + C_0\mu}, \tag{17}$$

with two constants, A and C_0. Fitting the line shape of the sharp peak in Fig. 8 given by filled circles revealed that $C_0 \approx 1.0$. This indicates that the self-energy of the X orbital for a small but finite μ on the real energy axis is obtained by shifting the self-energy of the half-filled system by $-\mu$ along the real energy axis, in accordance with the rigid-band model.

The triangles and crosses in Fig. 8 show the self-energy of the X orbital at ω_0 for two relatively large orbital mixing parameters, $v = 0.8t$ and t, respectively. For these values of v, the overlayer is metallic in the whole μ range. With increasing v, the sharp peak structure in $\mathrm{Im}\Sigma_{\mathrm{X}}(i\omega_0)$ as a function of μ is broadened. Including the real part shown in panel (a), when μ is small, the self-energy of the X orbital for a finite v may be expressed approximately by the form

$$\Sigma_{\mathrm{X}}(i\omega_n) \simeq \frac{U}{2} + \frac{A}{i(\omega_n + D) + C_0\mu}, \tag{18}$$

where the positive constant D increases with increasing v. As seen from Fig. 8(b), the X orbital has a finite low-frequency scattering rate,

$$\gamma_{\mathrm{X}} = -\lim_{\omega_n \to 0} \mathrm{Im}\Sigma_{\mathrm{X}}(i\omega_n),$$

in the range of μ corresponding to the energy gap of the isolated monolayer even for large values of the orbital mixing parameter v. According to Eq. (18), for small $|\mu|$ values, γ_{X} may be given by

$$\gamma_{\mathrm{X}} = \frac{AD}{D^2 + (C_0\mu)^2}. \tag{19}$$

For the outer regions of μ, where the isolated monolayer is metallic ($|\mu| > \mu_e$), the damping rate γ_{X} in Fig. 8(b) does not change significantly upon increasing v and decays with increasing $|\mu|$.

To illustrate the temperature dependence of the scattering rate, we display in Fig. 9 $\mathrm{Im}\Sigma_{\mathrm{X}}(i\omega_n)$ as a function of Matsubara frequency ω_n for two temperatures, $T = 0.01t$ and $0.04t$. For simplicity, we consider only the electron-hole symmetric case with $\mu = 0$. The orbital mixing parameter v for the four lines in each panel varies from 0 to t from top to bottom. For small ω_n, the ω_n dependence of these lines can be understood as a particular case of Eq. (18) with $\mu = 0$. It is seen that γ_{X} increases with decreasing temperature T. This result is in striking contrast to single-site DMFT calculations for metal/Mott insulator interfaces,[14,15] where the insulator becomes a Fermi liquid at low temperatures upon switching on orbital hybridizations between overlayer and substrate. Instead, we find here that, as a consequence of short-range fluctuations, the overlayer becomes bad-metallic due to strong non-Fermi-liquid properties.

The cluster components of the self-energy can be used to construct an approximate lattice self-energy by[19,26]

$$\Sigma(\mathbf{k},\omega) = \alpha_\Gamma\Sigma_\Gamma(\omega) + \alpha_{\mathrm{M}}\Sigma_{\mathrm{M}}(\omega) + \alpha_{\mathrm{X}}\Sigma_{\mathrm{X}}(\omega), \tag{20}$$

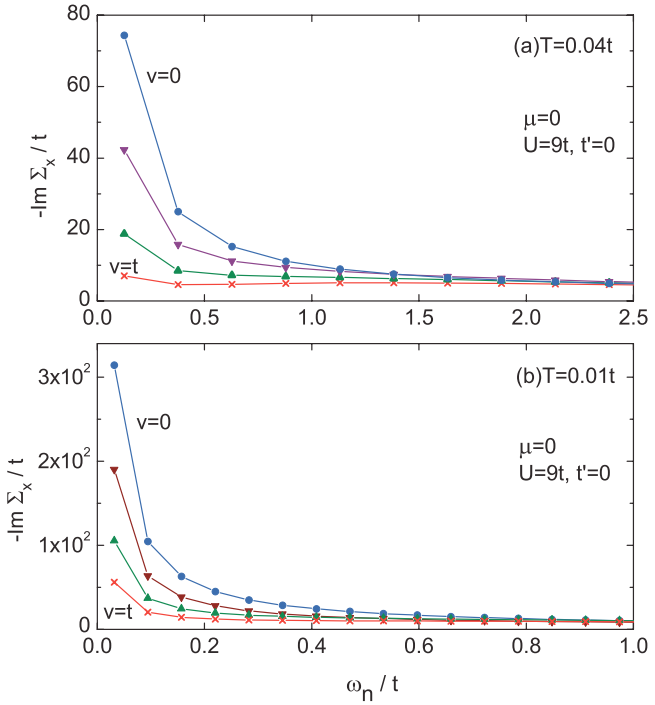

FIG. 9. (Color online) Imaginary part of the self-energy of the X orbital as a function of Matsubara frequencies ω_n for electron-hole symmetric systems with $\mu = 0$, $t' = 0$, and $U = 9t$. Four lines correspond to $v = 0$, $0.4t$, $0.8t$, and t (increasing from above). (a) $T = 0.04t$; (b) $T = 0.01t$.

where

$$\begin{aligned} \alpha_\Gamma &= (1+\cos k_x)(1+\cos k_y)/4, \\ \alpha_M &= (1-\cos k_x)(1-\cos k_y)4, \\ \alpha_X &= (1-\cos k_x \cos k_y)/2, \end{aligned} \tag{21}$$

with $-\pi \leqslant k_x, k_y \leqslant \pi$. Since the low-frequency damping rates of the Γ and M orbitals nearly vanish, as discussed above, we obtain a low-frequency damping rate at a general 2D wave vector,

$$\gamma(\mathbf{k}) = \frac{1-\cos k_x \cos k_y}{2}\gamma_X. \tag{22}$$

This equation, which exhibits strong anisotropy as a function of $\mathbf{k}$, holds true in the region of μ corresponding to the energy gap of the isolated monolayer and for a wide range of the orbital mixing parameter v ($0 < v \leqslant t$).

C. Transport properties

We calculate the in-plane dc conductivity of the adsorbed monolayer by using the Kubo formula,

$$\sigma_x = \frac{2e^2}{\pi\hbar}\int \frac{d\mathbf{k}}{(2\pi)^2}\left(\frac{\partial\epsilon(\mathbf{k})}{\partial k_x}\right)^2 [\mathrm{Im}G(\mathbf{k},\omega=0)]^2, \tag{23}$$

where $G(\mathbf{k},\omega)$ denotes the Green function of the periodized lattice, and the energy derivative of the Fermi distribution function, $\partial f/\partial\omega$, is approximated by $\delta(\omega)$ assuming that the integrand is a moderately varying function of ω. Okamoto *et al.*[37] have demonstrated that while Eq. (23) neglects vertex corrections, it reproduces rather well the conductivity

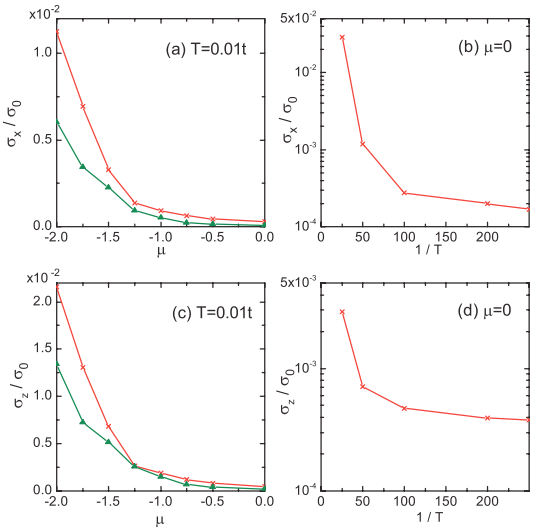

FIG. 10. (Color online) (a) In-plane conductivity of the overlayer, σ_x, as a function of μ at $T = 0.01t$, and (b) σ_x as a function of $1/T$ for half-filled systems with $\mu = 0.0$. (c) Out-of-plane conductance of the overlayer, σ_z, as a function of μ at $T = 0.01t$, and (d) σ_z as a function of $1/T$ for $\mu = 0.0$. $U = 9t$ and $t' = 0$ in all panels. Crosses and triangles correspond to two orbital mixing parameters, $v = t$ and $v = 0.8t$, respectively.

obtained by using the formulation of Lin *et al.*[38] where vertex corrections are included within the dynamical cluster approximation in DMFT. As in the work of Okamoto *et al.*,[37] we calculate the approximate periodic Green function of the lattice by

$$G(\mathbf{k},i\omega_n) = \frac{1}{4}\sum_{i,j=1}^{4} e^{i\mathbf{k}\cdot(\mathbf{x}_i-\mathbf{x}_j)}G_{ij}(i\omega_n), \tag{24}$$

where $G_{ij}(i\omega_n)$ denotes the cluster Green function defined by Eq. (5). To evaluate its value at $\omega = 0$, we used a quadratic extrapolation of the values of $G_{ij}(i\omega_n)$ at the first three Matsubara frequencies.

In Fig. 10(a), we plot σ_x in units of $\sigma_0 = 2e^2/h$ for a range of μ corresponding to the lower half of the original Mott energy gap, where $U = 9t$, $t' = 0$, and $T = 0.01t$. Triangles and crosses correspond to $v = 0.8t$ and $v = t$, respectively. We note that σ_x for the insulating monolayer with $v = 0$ vanishes in the energy gap. It is seen that the calculated σ_x decreases as μ approaches the center of the energy gap $\mu = 0$. This behavior can be understood from the μ dependence of the imaginary part of the self-energy of the X orbital in the low-frequency limit. As discussed in the preceding subsection, its low-frequency scattering rate, γ_X, exhibits a large peak structure centered at $\mu = 0$ as a function of μ, which leads to the reduction of the spectral function in the low-frequency limit, $A(\mathbf{k},0) = -\pi^{-1}\mathrm{Im}G(\mathbf{k},\omega=0)$, appearing in Eq. (23) and thus to a concomitant decrease in σ_x.

In Fig. 10(b), we show the temperature variation of σ_x at half-filling with the hybridization parameter $v = t$. In the preceding subsection, we have shown that γ_X increases as the temperature decreases from $T = 0.04t$ to $0.01t$. Extending these calculations to even lower T, we find that γ_X continues to increase with decreasing temperature down to $T \sim t/300$.

The temperature range below $T < t/300$ was not investigated, since in the present exact diagonalization scheme, the fitting of the Green function in Eq. (11) becomes more difficult as the lowest Matsubara frequencies get closer to the real energy axis with decreasing T. In accord with the increase in γ_X with decreasing temperature, the calculated σ_x in Fig. 10(b) is seen to decrease with decreasing T.

One may also be interested in the out-of-plane transport. As seen from Eq. (6), the electronic structure of the present overlayer system is exactly the same as that of a monolayer film sandwiched between two semi-infinite noninteracting substrates for which the coupling constant v between the monolayer and each substrate is reduced by factor $\sqrt{2}$. The conductance of such a sandwiched film in the normal direction is given at low temperature and in the zero-bias limit by[17,39]

$$\sigma_z = \frac{2e^2}{h} \int \frac{d\mathbf{k}}{(2\pi)^2} [2\,\mathrm{Im}s(\mathbf{k},\mu)]^2 \, |G(\mathbf{k},\omega=0)|^2, \quad (25)$$

where $s(\mathbf{k},\mu)$ denotes the embedding potential of the leads on both sides. We assume that the right and left leads are the same and coupled with the sandwiched monolayer with mixing parameter $v/\sqrt{2}$ as mentioned above. Also, it is to be noted that the integrand of Eq. (25) has a physical meaning as electron transmittance probability in the noninteracting limit. We show in Figs. 10(c) and 10(d) the calculated σ_z as a function of μ at $T = 0.01t$ and as a function of $1/T$ at half-filling ($\mu = 0$), respectively. The other parameters are the same as in panels (a) and (b). While Eq. (23) for σ_x contains the imaginary part of the lattice Green function in its integrand, Eq. (25) for σ_z contains the absolute value of the Green function. In spite of this difference, the characteristic features of the calculated μ and T dependence of σ_z shown in Figs. 10(c) and 10(d) are very similar to those of σ_x in panels (a) and (b).

D. Effect of the second neighbor interaction t': First-order metal-to-metal transition

Having understood the physics involved in the systems with $t' = 0$, we now consider the case in which the second nearest-neighbor hopping interaction t' is nonvanishing. Specifically, we choose t' as $t' = -0.3t$. As shown in Fig. 2(d), upon introducing a finite t' value, the van Hove singularity in the noninteracting DOS shifts to the hole-doping side for the isolated monolayer with $v = 0$. With increasing v, this peak in the DOS becomes gradually blurred.

In Fig. 11, we show $n(\mu)$ and $-G_{ii}(\beta/2)$ as a function of chemical potential μ for $v = 0$, $v = 0.8t$, and $v = t$, where we adopt again the parameters $U = 9t$ and $T = 0.04t$. As in Fig. 3, $n(\mu)$ for the isolated monolayer exhibits a plateau in the Mott insulating phase. Correspondingly, $-G_{ii}(\beta/2)$ for $v = 0$ vanishes in the region of μ, which is slightly narrower than the Mott gap. The metal-insulator transition on the hole-doping side is continuous. On the other hand, in contrast to the case of $t' = 0$, the transition on the electron-doping side reveals a hysteresis, which agrees with the previous cluster DMFT work.[26] As in the case of $t' = 0$, the overlayer is metallized when it is coupled to the metal substrate via the proximity effect. It is seen that the plateau in $n(\mu)$ disappears and the compressibility $(dn/d\mu)_T$ becomes positive in the entire μ range for $v = 0.8t$ and $v = t$.

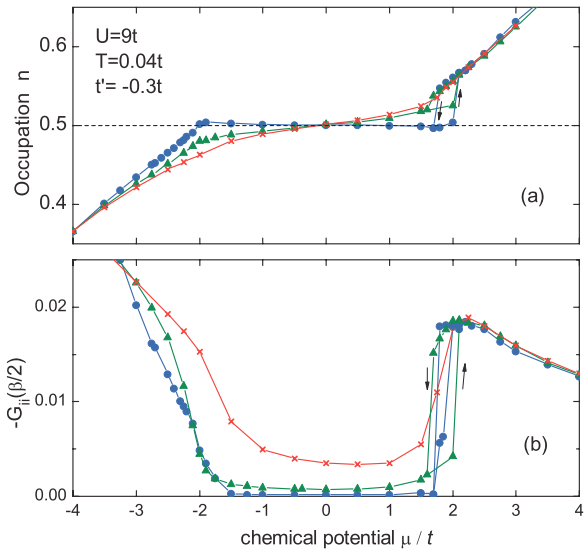

FIG. 11. (Color online) (a) Electron occupation per spin and (b) integrated spectral weight around chemical potential, $-G_{ii}(\beta/2)$, of an overlayer site as a function of chemical potential μ derived within four-site cluster DMFT. $U = 9t$, $T = 0.04t$, and $t' = -0.3t$. Filled circles, triangles, and crosses correspond to substrate-adatom hybridizations, $v = 0$, $v = 0.8t$, and $v = t$, respectively.

In addition, for $v = 0.8t$, $\mu \approx 2t$ (electron doping), $n(\mu)$ shows a similar hysteresis as for $v = 0$. This behavior demonstrates that, at moderate coupling to the substrate, the overlayer exhibits two metallic phases separated by a first-order phase transition. As seen from Fig. 11(b), the integrated quasiparticle DOS around the chemical potential in the μ range corresponding to the original Mott gap is very small, indicating that the metallic phase in the original gap is much more strongly correlated than the second metallic phase beyond the gap. The origin of this strongly reduced quasiparticle DOS is the large low-frequency scattering rate of the X orbital as discussed in Sec. III B. To show that this holds also for $t' = -0.3t$, we plot in Fig. 12 the real and imaginary parts of the self-energy of the X orbital at the first Matsubara frequency ω_0 as a function of μ. The qualitative behavior of the self-energy is seen to be very similar to that in Fig. 8: For $v = 0.8t$, $\mathrm{Im}\Sigma_X(i\omega_0)$ exhibits a pronounced peak structure inside the original gap. If the interaction with the substrate is increased to $v = t$, metallicity in the overlayer is further enhanced and the first-order transition between these metallic phases is replaced by a continuous one. For hole doping, $n(\mu)$ varies smoothly, regardless of the value of v.

E. Discussion

Before closing this section, we discuss several issues concerning the metallization of the overlayer. As shown in Fig. 2, the single-particle DOS of the overlayer site is broadened with increasing orbital mixing parameter v. We emphasize, however, that the metallization of the overlayer cannot be explained in terms of such a broadening of the DOS alone. To demonstrate this, we calculated the electronic

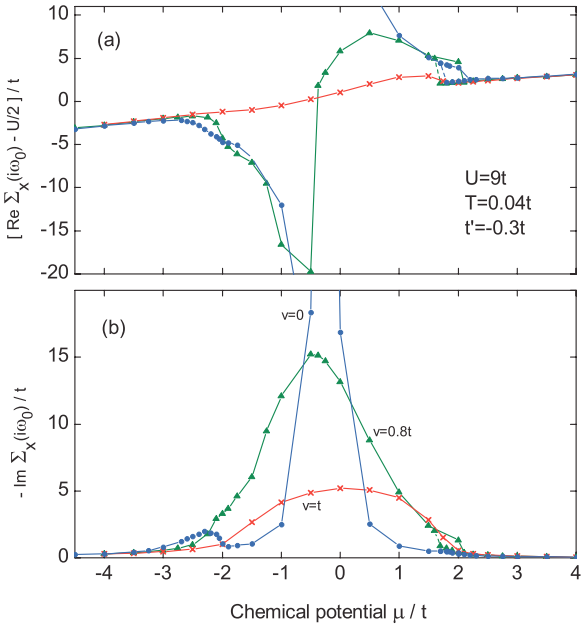

FIG. 12. (Color online) (a) Real and (b) imaginary parts of the self-energy of the X orbital at the first Matsubara frequency $\omega_0 = \pi T$ for $v = 0$ (filled circle), $v = 0.8t$ (triangle), and $v = t$ (cross). $U = 9t$, $T = 0.04t$, and $t' = -0.3t$.

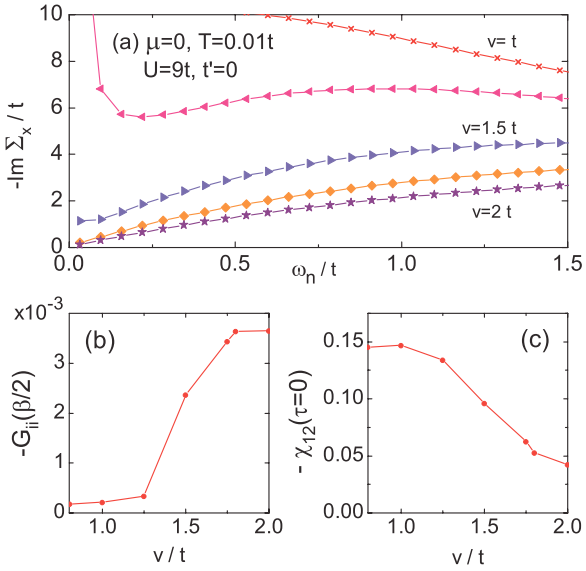

FIG. 13. (Color online) (a) Imaginary part of the self-energy of the X orbital as a function of ω_n for large orbital mixing parameters. Five lines correspond to $v = t$, $1.25t$, $1.5t$, $1.75t$, and $2t$ from top to bottom. (b) Integrated spectral weight around μ, $-G_{ii}(\beta/2)$, and (c) spin correlation function $\chi_{12}(\tau = 0)$ for large v/t values. In all panels, $\mu = 0$, $t' = 0$, $U = 9t$, and $T = 0.01t$.

structure of model monolayers by applying the single-site DMFT and the expression of the interacting Green function,

$$G(i\omega_n) = \int d\epsilon \, \frac{\rho_0(\epsilon)}{i\omega_n + \mu - \epsilon - \Sigma(i\omega_n)}, \tag{26}$$

where $\rho_0(\epsilon)$ denotes the single-particle DOS given in Fig. 2. We chose $U = 12t$ instead of $U = 9t$, as critical Coulomb energies in single-site DMFT are considerably larger. It was found that the monolayer becomes a Mott insulator at half-filling not only for the DOS curves in Figs. 2(a) and 2(d), which exhibit van Hove singularities, but also for the broader ones in the lower four panels.

On the other hand, the true overlayers on a metallic substrate become metallic for the same Coulomb repulsion energy in both single-site DMFT (see the Appendix) and cluster DMFT calculations. What is essential for the metallization of the overlayer is the embedding potential of the metallic substrate. We note that Eq. (26), which is valid for a single-band system within single-site DMFT, does not hold for the overlayer system. Generally, the Green function of the overlayer is given by

$$G(i\omega_n) = \sum_{\mathbf{k}} G(\mathbf{k}, i\omega_n) \tag{27}$$

and

$$G(\mathbf{k}, i\omega_n) = [i\omega_n + \mu - \epsilon(\mathbf{k}) - \Sigma(\mathbf{k}, i\omega_n) - s(\mathbf{k}, i\omega_n + \mu)]^{-1}, \tag{28}$$

where $-\pi \leqslant k_x, k_y \leqslant \pi$. The embedding potential $s(\mathbf{k},\omega)$ has a finite imaginary part when real frequency ω lies within the energy continuum of the substrate band at a given $\mathbf{k}$. This necessarily gives rise to a nonvanishing value of the $\mathbf{k}$-resolved spectral function $A(\mathbf{k},\omega) = -\pi^{-1}\mathrm{Im}G(\mathbf{k},\omega)$, as long as the correlation-induced self-energy $\Sigma(\mathbf{k},\omega)$ in Eq. (28) does not diverge. We have shown in the preceding subsections that the self-energy diverges only for the isolated monolayer ($v = 0$) at half-filling. Thus, as long as the chemical potential μ lies in the energy continuum of the projected substrate band in a finite portion of the surface Brillouin zone, the system has a finite quasiparticle DOS at μ, i.e., the overlayer is metallic.

So far, we varied the overlayer-substrate orbital hybridization strength between $0 \leqslant v \leqslant t$ and demonstrated that the overlayer becomes a bad metal in a wide parameter range as a function of chemical potential and temperature. While it seems to be unlikely that the hopping interaction between the overlayer and substrate sites in realistic systems exceeds those between first nearest neighbors in the overlayer or in the substrate, it is intriguing from a theoretical point of view to investigate whether the overlayer undergoes a phase transition from a non-Fermi-liquid to a Fermi-liquid state at some critical v value, when the orbital mixing parameter v is increased. To examine this issue, we performed additional cluster DMFT calculations for several overlayer systems for v values larger than t.

In Fig. 13(a), we show the imaginary part of the self-energy of the X orbital as a function of ω_n for five v values. The system is electron-hole symmetric ($t' = 0$ and $\mu = 0$), and the parameters, $U = 9t$ and $T = 0.01t$, are the same as those in $\mathrm{Im}\Sigma_X(i\omega_n)$ in Fig. 9(b). Because of the large difference in the vertical axis scale, we have chosen to plot Fig. 13(a) separately from Fig. 9(b). From these two plots, one clearly sees that $\mathrm{Im}\Sigma_X(i\omega_n)$ changes drastically with increasing orbital mixing parameter v. The system is a Mott insulator at $v = 0$ while it becomes a bad metal for $v \leqslant t$, as discussed in the preceding subsections. As seen in Fig. 13(a), when v is increased further, the overlayer is finally turned into a Fermi liquid at $v \sim 1.75t$, where $\mathrm{Im}\Sigma_X(i\omega_n)$ varies linearly with ω_n and

vanishes in the low-frequency limit. In Figs. 13(b) and 13(c), we plotted $-G_{ii}(\beta/2)$ and $-\chi_{12}(\tau=0)$ for these large v values, respectively. It is seen that the spectral weight in the Fermi-liquid phase grows rapidly while antiferromagnetic spin ordering between nearest-neighbor sites is greatly reduced as the overlayer enters a Fermi-liquid phase with increasing v. We also performed calculations for large v values in the electron-hole asymmetric system with $U=9t$ and $t'=-0.3t$ and found a similar critical value, $v\sim 1.75t$, for the transition from non-Fermi-liquid to Fermi-liquid behavior. It is unlikely that such a large hybridization strength occurs in realistic materials. Thus, in heterostructures, we expect cuprate superconductors in the normal state to be a bad metal when placed in contact with a weakly correlated metal.

In contrast, within single-site DMFT, the overlayer becomes a Fermi liquid at much smaller v values when v is increased from zero. For example, for the electron-hole symmetric overlayer with a large Coulomb energy, $U=12t$, the critical v value at $T=0.01t$ is only $\sim 0.6t$ (see the Appendix). This indicates that short-range Coulomb correlations included in the cluster DMFT strongly reduce the metal proximity effect, and, as a result, greatly increase the critical coupling strength for the transition from non-Fermi-liquid to Fermi-liquid behavior at a given temperature as compared with that in single-site DMFT.

As shown above, the overlayer at a given temperature becomes a Fermi liquid if v is assumed to be arbitrarily large. Another interesting question is whether the overlayer at moderate coupling $v\leqslant t$ becomes a Fermi liquid at very low temperatures. As discussed in Sec. III C, for $v=t$ the overlayer remains a bad metal even at $T\sim t/300$, whereas in single-site DMFT it is a Fermi liquid at $T=0.04t$ (see the Appendix). This might suggest that the effective Fermi temperature, T_F, below which the overlayer exhibits Fermi-liquid properties, is greatly reduced as a consequence of short-range spatial fluctuations. The present results indicate that $T_F<t/300$ for $v=t$. It would be interesting to clarify whether the overlayer with $v\leqslant t$ exhibits a finite T_F or whether it remains a bad metal down to $T=0$. Since finite-size effects limit the range of accuracy of exact diagonalization at very low temperatures, this issue must be left as an open question.

IV. SUMMARY

We have studied the electronic structure of the interface between a Mott insulating monolayer and a semi-infinite noninteracting metal substrate by applying dynamical mean-field theory. In order to incorporate the effects of short-range interatomic correlations in the plane, we performed four-site cluster DMFT calculations. We have investigated how the overlayer is metallized when it is coupled with the substrate via orbital hybridization. While the 2D Mott insulating overlayer becomes metallic in both single-site and cluster DMFT calculations, there is an essential difference in the electronic properties of the metallized overlayer: Within the single-site approximation, the overlayer exhibits Fermi-liquid properties at low temperatures, whereas short-range Coulomb correlations induce bad-metallic behavior in the overlayer in a much wider parameter range than expected from single-site DMFT. The self-energy component representing approximately the $(\pi,0)$ sector of the 2D Brillouin zone then exhibits a finite low-frequency scattering rate, which increases with decreasing temperature, even when the orbital hybridization between overlayer and substrate sites is as large as the nearest-neighbor hopping energy inside the overlayer. This leads to a strong anisotropy of the scattering rate of electrons on the Fermi surface in the surface Brillouin zone. In addition, we have shown that the first-order metal-insulator transition of the isolated overlayer (for electron doping in the presence of second-neighbor hopping) is converted into a first-order transition between strongly and weakly correlated metallic phases. In agreement with our previous work for sandwiched films,[17] the present results suggest that the normal metal proximity effect is strongly reduced when spatial fluctuations in the overlayer are taken into consideration.

ACKNOWLEDGMENTS

H.I. thanks the Alexander von Humboldt Foundation for support during his stay in Germany. The work of H.I. was supported by a Grant-in-Aid for Scientific Research (No. 20540191) from the Japan Society for the Promotion of Science.

APPENDIX: SINGLE-SITE DMFT

For comparison with the cluster DMFT results discussed above, we have also performed single-site DMFT calculations for the Mott insulating overlayer in contact with a metal substrate. Since critical Coulomb energies in a local picture are considerably larger, we take $U=12t$ to ensure that the isolated overlayer at half-filling is a Mott insulator. We show only the results for $t'=0$, since those for $t'=-0.3t$ are qualitatively very similar.

Figure 14 shows $n(\mu)$ as a function of μ for $v=0$, $v=0.8t$, and $v=t$. For the isolated monolayer, we find a plateau $n(\mu)=0.5$ in the interval $\mu_h\leqslant\mu\leqslant\mu_e$ with $|\mu_h|=|\mu_e|\approx 1.75t$, where the monolayer is insulating. For finite v values, the plateau in $n(\mu)$ is replaced by a smoothly increasing variation, consistent with the metallization of the overlayer. Although one can still identify a more strongly correlated metallic phase in the range of the original Mott gap of the

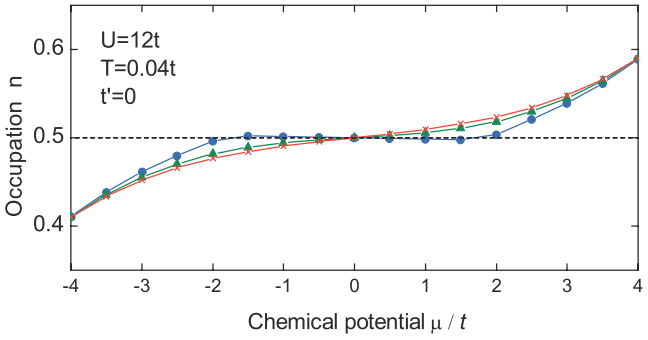

FIG. 14. (Color online) Electron occupation per spin of an overlayer site as a function of chemical potential, calculated within single-site DMFT. $U=12t$, $T=0.04t$, and $t'=0$. Solid circles, triangles, and crosses correspond to $v=0$, $v=0.8t$, and $v=t$, respectively.

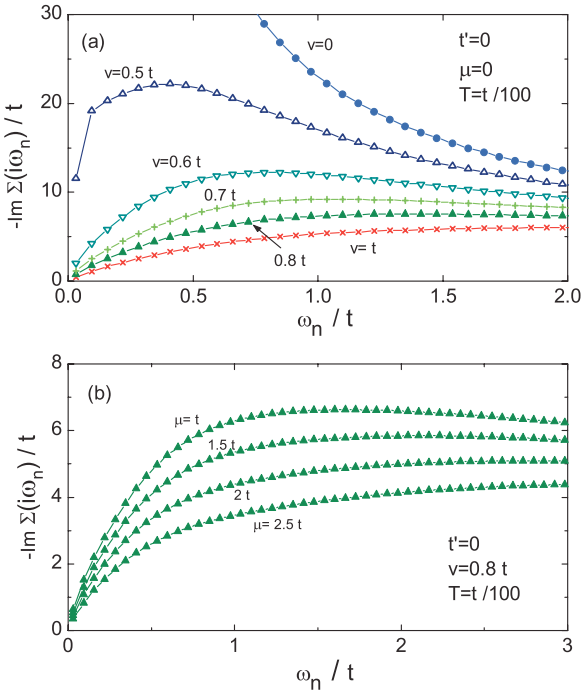

FIG. 15. (Color online) (a) Imaginary part of overlayer self-energy, calculated within single-site DMFT at half-filling, for $t' = 0$, $U = 12t$, and $T = 0.01t$. The overlayer-substrate coupling increases from $v = 0$ to $v = t$. (b) Same as (a) except for increasing chemical potential, $\mu = t, \ldots, 2.5t$, at fixed overlayer-substrate coupling $v = 0.8t$.

isolated monolayer, the transition to the weakly correlated region at larger electron or hole doping in the local DMFT is seen to be much more gradual than in the presence of short-range fluctuations (see Figs. 3 and 11). Moreover, there is no evidence for a first-order transition, including the case of electron doping for $v = 0.8t$ and $t' = -0.3t$ (not shown).

Figure 15(a) shows the imaginary part of the overlayer self-energy for several values of the adatom substrate coupling v. For simplicity, we consider the electron-hole symmetric case with $\mu = 0$ and $t' = 0$. Also, to clarify the low-frequency properties of the self-energy, we choose a lower temperature $T = 0.01t$. For the isolated layer ($v = 0$), $\mathrm{Im}\Sigma(i\omega_n) \sim 1/\omega_n$

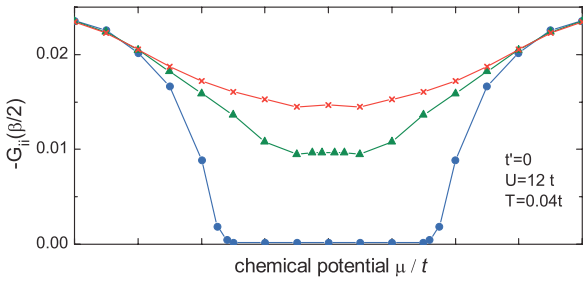

FIG. 16. (Color online) Integrated spectral weight near the chemical potential, $-G_{ii}(\beta/2)$, of an overlayer site as a function of μ within single-site DMFT. $U = 12t$, $T = 0.04t$, and $t' = 0$. Filled circles, triangles, and crosses correspond to substrate-adatom hybridizations, $v = 0$, $v = 0.8t$, and $v = t$, respectively.

in the limit of $\omega_n \to 0$, indicating that the layer is a Mott insulator. For a relatively small mixing parameter $v = 0.5t$, the condition $T \ll T_F$ (effective Fermi temperature) apparently does not hold. As a result, $\mathrm{Im}\Sigma(i\omega_n)$ tends to a finite value as $\omega_n \to 0$, suggesting that the overlayer is a bad metal. For $v \geqslant 0.6t$, $\mathrm{Im}\Sigma(i\omega_n) \sim \omega_n$ at small ω_n, indicating that the overlayer is in a Fermi-liquid phase. To illustrate the effect of electron doping, we show in Fig. 15(b) the imaginary part of the overlayer self-energy for various chemical potentials at fixed $v = 0.8t$. Since $\mathrm{Im}\Sigma(i\omega_n) \sim \omega_n$ at low ω_n, the overlayer is a Fermi liquid, with increasing quasiparticle weight for increasing doping. Also, these curves vary smoothly across the metal-insulator boundary of the isolated monolayer, $\mu_e \approx 1.75t$. This behavior, obtained within local DMFT, suggests that, in contrast to the isolated monolayer, and in contrast to the cluster DMFT treatment as a result of the coupling to the substrate, the overlayer does not undergo a phase transition as a function of μ.

The Fermi-liquid behavior of the metallized overlayer can also be clearly seen from the integrated spectral weight near the chemical potential, $-G_{ii}(\beta/2)$, as shown in Fig. 16 for the overlayers corresponding to Fig. 14. In striking contrast to Fig. 3 obtained by using the cluster DMFT, $-G_{ii}(\beta/2)$ within single-site DMFT grows rapidly in the original gap region with increasing v, which originates from the quasiparticle DOS peak at μ (Kondo peak) in the Fermi-liquid phase.

[1] A. Ohtomo, D. A. Muller, J. L. Grazul, and H. Y. Hwang, Nature (London) **419**, 378 (2002).
[2] A. Ohtomo and H. Y. Hwang, Nature (London) **427**, 423 (2004).
[3] T. Yajima, Y. Hikita, and H. Y. Hwang, Nat. Mater. **10**, 198 (2011).
[4] S. Okamoto and A. J. Millis, Nature (London) **428**, 630 (2004).
[5] T. Oka and N. Nagaosa, Phys. Rev. Lett. **95**, 266403 (2005).
[6] E. Dagotto, Science **318**, 1076 (2007).
[7] J. K. Freericks, V. Zlatić, and A. M. Shvaika, Phys. Rev. B **75**, 035133 (2007).
[8] S. Yunoki, A. Moreo, E. Dagotto, S. Okamoto, S. S. Kancharla, and A. Fujimori, Phys. Rev. B **76**, 064532 (2007).
[9] S. Okamoto, Phys. Rev. Lett. **101**, 116807 (2008).
[10] N. Reyren, S. Thiel, A. D. Caviglia, L. F. Kourkoutis, G. Hammerl, C. Richter, C. W. Schneider, T. Kopp, A.-S. Rüetschi, D. Jaccard, M. Gabay, D. A. Muller, J.-M. Triscone, and J. Mannhart, Science **317**, 1196 (2007).
[11] H. W. Jang, D. A. Felker, C. W. Bark, Y. Wang, M. K. Niranjan, C. T. Nelson, Y. Zhang, D. Su, C. M. Folkman, S. H. Baek, S. Lee, K. Janicka, Y. Zhu, X. Q. Pan, D. D. Fong, E. Y. Tsymbal, M. S. Rzchowski, and C. B. Eom, Science **331**, 886 (2011).
[12] A. Georges, G. Kotliar, W. Krauth, and M. J. Rozenberg, Rev. Mod. Phys. **68**, 13 (1996).
[13] For recent reviews, see K. Held, Adv. Phys. **56**, 829 (2007); G. Kotliar, S. Y. Savrasov, K. Haule, V. S. Oudovenko, O. Parcollet, and C. A. Marianetti, Rev. Mod. Phys. **78**, 865 (2006).
[14] R. W. Helmes, T. A. Costi, and A. Rosch, Phys. Rev. Lett. **101**, 066802 (2008).

[15]H. Zenia, J. K. Freericks, H. R. Krishnamurthy, and Th. Pruschke, Phys. Rev. Lett. **103**, 116402 (2009).
[16]M. Potthoff and W. Nolting, Phys. Rev. B **59**, 2549 (1999); **60**, 7834 (1999).
[17]H. Ishida and A. Liebsch, Phys. Rev. B **82**, 045107 (2010).
[18]G. Kotliar, S. Y. Savrasov, G. Pálsson, and G. Biroli, Phys. Rev. Lett. **87**, 186401 (2001).
[19]M. Civelli, M. Capone, S. S. Kancharla, O. Parcollet, and G. Kotliar, Phys. Rev. Lett. **95**, 106402 (2005).
[20]B. Kyung, S. S. Kancharla, D. Sénéchal, A. M. S. Tremblay, M. Civelli, and G. Kotliar, Phys. Rev. B **73**, 165114 (2006).
[21]H. Park, K. Haule, and G. Kotliar, Phys. Rev. Lett. **101**, 186403 (2008).
[22]A. Macridin and M. Jarrell, Phys. Rev. B **78**, 241101(R) (2008).
[23]P. Werner, E. Gull, O. Parcollet, and A. J. Millis, Phys. Rev. B **80**, 045120 (2009).
[24]S. Sakai, Y. Motome, and M. Imada, Phys. Rev. Lett. **102**, 056404 (2009).
[25]N. S. Vidhyadhiraja, A. Macridin, C. Sen, M. Jarrell, and M. Ma, Phys. Rev. Lett. **102**, 206407 (2009).
[26]A. Liebsch and N.-H. Tong, Phys. Rev. B **80**, 165126 (2009).
[27]E. Gull, M. Ferrero, O. Parcollet, A. Georges, and A. J. Millis, Phys. Rev. B **82**, 155101 (2010).
[28]G. Sordi, K. Haule, and A.-M. S. Tremblay, Phys. Rev. Lett. **104**, 226402 (2010).
[29]J. E. Inglesfield, Comput. Phys. Commun. **137**, 89 (2001).
[30]H. Ishida and A. Liebsch, Phys. Rev. B **79**, 045130 (2009).
[31]D. Kalkstein and P. Soven, Surf. Sci. **26**, 85 (1971).
[32]M. Caffarel and W. Krauth, Phys. Rev. Lett. **72**, 1545 (1994).
[33]C. A. Perroni, H. Ishida, and A. Liebsch, Phys. Rev. B **75**, 045125 (2007).
[34]A. Liebsch, H. Ishida, and J. Merino, Phys. Rev. B **79**, 195108 (2009).
[35]A. Liebsch, Phys. Rev. B **83**, 035113 (2011).
[36]R. B. Lehoucq, D. C. Sorensen, and C. Yang, *ARPACK Users' Guide* (SIAM, Philadelphia, 1997).
[37]S. Okamoto, D. Sénéchal, M. Civelli, and A.-M. S. Tremblay, Phys. Rev. B **82**, 180511(R) (2010).
[38]N. Lin, E. Gull, and A. J. Millis, Phys. Rev. B **80**, 161105(R) (2009).
[39]Y. Meir and N. S. Wingreen, Phys. Rev. Lett. **68**, 2512 (1992).